ON THE MICROSTRUCTURAL CHARACTERISTICS OF NON-EQUILIBRIUM GAMMA-PRECIPITATES IN Cu-Zn-Al ALLOYS

F.C. Lovey[(a)] and E. Cesari[(b)]

(a) División Metales, Céntro Atómico Bariloche, 8400 San Carlos de Bariloche, Argentina.

(b) Dept. de Física, Facultat de Ciencias, Crtra. Valldemossa km. 7.5, Universitat de les Illes Balears, 07071 Palma de Mallorca, Spain.

ABSTRACT

The characteristics of the martensitic transformations can be greatly influenced by the presence of a second phase precipitates in the matrix. The interaction of the martensite with the precipitates depends strongly on the precipitate features. The microstructural characteristics of γ precipitates in the β matrix in a Cu-Zn-Al alloy is studied in this work. The analysis is performed by transmission electron microscopy and results concerning the precipitate morphology, size, distribution and degree of coherency are reported. The kinetics of the precipitate growth follows the Ostwald ripening mechanism and the biggest precipitates are semicoherent encircled by <100> edge type dislocation loops.

1. INTRODUCTION

The effect of γ-precipitates on the martensitic transformation in Cu-Zn-Al alloys has been the subject of recent studies. The presence of such precipitates was found to produce several changes in the characteristics of the martensitic transformation [1-4]: shift of the M_s temperature, increase of the hysteresis width and of the Ms-Mf difference, etc..

Precipitates of the γ-phase can be produced in the β-phase matrix of Cu-Zn-Al alloys by a variety of thermal treatments [1-6]. Thus for example small precipitates can be obtained by quenching from a temperature Tq between 670 and 970 K into water at a temperature Tw < 320 K [5]. The size and distribution of the precipitates depend on the temperature Tq. These precipitates are formed during the quenching procedure under non-equilibrium conditions. They can be made to grow by further ageing for short times at temperatures between 520 and 770 K [2,7].

The knowledge of the characteristics of the precipitates is important to understand the interaction mechanisms with the martensitic transformation [4]. In this work several microstructural aspects of the γ-precipitates such as their size, morphology and the analysis of interface dislocations, obtained by particular thermal treatments, are studied by transmission electron microscopy.

2. EXPERIMENTAL PROCEDURE

A single crystal of Cu-16.3 Al-15.3 Zn (at%) was used. The γ-precipitates were produced by the following thermal treatments. After homogeneization at 1120 K the specimen was air cooled to 770 K, held there for 3 minutes, and then quenched into ice water.

Small γ-type precipitates are formed during quenching [5,6]. These precipitates were made to grow to different sizes by ageing at 670 K for variable times (t^*).

Thin foils for electron microscopy were prepared by initial jet polishing with an electrolyte solution consisting of 25% phosphoric acid and 25% methanol in water, followed by a final electropolishing procedure in a saturated solution of chromium trioxide in phosphoric acid at 1.5 V. The samples were observed with a 100 kV Hitachi electron microscope.

3. RESULTS AND DISCUSSION

3.1. Kinetics of the γ-precipitation.

Small cuboidal precipitates, as shown in Fig. 1 were observed in these samples in agreement with earlier reported results [5-6]. The size of the precipitates in Fig. 1 varies from 10 to 20 nm. Selected area diffraction patterns confirmed that the precipitates have a I-type γ-brass lattice. The spot distribution was however incommensurate, also in agreement with previous findings [5-7]. According to Lovey at al. [7] this incommensurability arises from the presence of small non periodic antiphase domains of the γ-brass superstructure in the precipitate.

It was also confirmed that the precipitates are coherent with the matrix, with a vacancy type of strain field, as reported by Rapacioli et al. [5]. This is observed in Fig. 1 where the g diffraction vector points towards the white lobe in the dark field black-white contrast.

The "basket" type microstructure observed in the matrix of Fig. 1 is due to surface effects (surface oxidation plus surface relaxation and surface martensite) as suggested by Van Tendeloo et

al. [8,9] and it is not related to the precipitation or the particular thermal treatment.

3.1.2. Precipitates after flash heating to 673 K for 10 s

After ageing at 673 K for 10 s the precipitates do not show any significant change as compared to the as quenched state.

3.1.3. Precipitates after flash heating to 673 K for 20 s

After this thermal treatment the precipitates show the following changes (see Fig. 2a): i) Their sizes increase to a medium size of $\bar{r}$ = 62 nm, with a size distribution given in Fig. 2b, where ρ is the precipitate density. ii) Superlattice reflections appear in the diffraction patterns corresponding to a P-type cell, and all superlattice spots become commensurate with the fundamental reflections.

The precipitate remains cuboidal with {100} habit and they are coherent with the matrix giving a vacancy type strain field in the dark field image of Fig. 2a.

3.1.4. Precipitates after flash heating to 673 K for 40 s

The bright field image in Fig. 3a shows an increase of the precipitate size to a medium size of 120 nm. The corresponding size distribution is shown in Fig. 3b. Some striations are observed inside the precipitate images which are parallel to the cubic edges ({100} habit). Later on (paragraph 3.2) it will be shown that these striations are the images of interface dislocations with <100> Burgers vectors. Thus, after ageing at 673 K for 40 s the precipitates start loosening their coherency with one or two dislocations in the 120 nm width.

3.1.5. Precipitates after flash heating to 673 K for 60 s

After this thermal treatment the precipitates are still rather cuboidal, although they tend to be more polyhedral, as shown in Fig. 4a. Some interface dislocations are observed. The medium size is $\bar{r}$ = 130 nm and the size distribution is given in Fig. 4b. A comparison between Fig. 3b and 4b shows that the latter distribution is slightly wider and more asymmetric than the former.

3.1.6. Precipitates after flash heating to 673 K for 100 s

The precipitates distribution is shown in Fig. 5a. The asymmetry and wideness of the size distribution increases as compared to the previous thermal treatments: this can be deduced by comparing Fig. 5b with 4b and 3b respectively. The medium size is $\bar{r}$ = 166 nm. It is seen in Fig. 5a that the precipitates are polyhedral with facets parallel to {100} and {110}. Chains of precipitates along the {100} directions are observed. The interface dislocations cross from one precipitate to the next aligned along the chain(s) (see also Fig. 6). The average density of dislocations is of one dislocation every 40 nm along the precipitate width.

The kinetics of the precipitate growth is consistent with the diffusion controlled mechanisms proposed by Lifshitz and Slyozov [10] and Wagner [11]. A linear relationship between $\bar{r}^3$ and the ageing time t* is found, as shown in Fig. 7. In addition to this, the Ostwald ripening is evident in Figs. 5a, b and also Fig. 6, where the larger precipitates grow at the expense of smaller ones.

The asymmetry of the size distribution (Figs. 4b and 5b) is also in qualitative agreement with the prediction of Lifshitz and Slyozov. The shape of the precipitates evolves from cuboidal with {100} habit to polyhedral with {100} and {110} facets as the ageing time (t^*) increases. This is probably associated with the relationship between the interfacial energy, the elastic energy due to the misfit of the lattices, and the interaction energy between precipitates [12]. The evaluation of these energies is rather difficult and this will not be performed here.

3.2. Analysis of the interface dislocations

The fringes observed in the precipitate images can be due to either Moiré fringes or interface dislocations. Both phenomena arise from a difference in the lattice constant between the matrix and precipitates. In addition neighbouring precipitates are some times connected by lines with dark contrast crossing through the matrix, see for example the central part of Figs. 6a to 6c showing two connected precipitates (A and B). This suggests that such contrast could be due to dislocations. The orientations of the line directions of these dislocations when embedded in the matrix is <010>. The contrast of these dislocations goes to extinction under bright field two beam conditions for the 020 diffraction spot, as shown in Fig. 6d. Owen to the high anisotropy of the β matrix this extinction can only occur for edge dislocations with Burgers vector $\vec{b} = a_\beta$ [100] [13].

The dislocation lines joining the precipitates A and B continue inside the precipitate images as observed in Fig. 6c. The contrast of these dislocations in the precipitates also disappears completely for the 020 diffraction vector (Fig. 6d),

suggesting that the invisibility criteria of Head et al [13] also follows for the <100> edge dislocations located along the precipitate-matrix interface. This can be understood as follows: the facets of the precipitates are essentially {100} and {110}, the line of the dislocation loops encircling the precipitates are alternatively parallel to <010> and <1$\bar{1}$0> directions. Regarding the matrix, these directions are perpendicular to a symmetry plane of the crystal and the invisibility criteria of Head et al. [13] can be applied. In the γ precipitates these symmetries are absent because of the lack of inversion center. Hence, it is not clear how the contrast would behave. From the experimental observation, we assume that the contribution of the deformation of the γ phase to the disloction contrast (for edge dislocations and g.b = 0) is also weak.

The fringes observed in Fig. 6a and b have a zig-zag shape, but on the average they are perpendicular to the diffraction vector, this is a characteristic of the Moiré fringes due to the lattice misfit [14,15]. The local position of the Moiré fringes is very sensitive to the presence of interface steps and interface dislocations [14,15], this can give an explanation of the wavy aspect of the fringes observed in Fig. 6a and b. In Fig. 6c and d there are weaker lines in between the stronger ones (the dislocations), these are Moiré fringes. In addition, it could be confirmed, by carefully tilting the specimen, that there are also Moiré fringes close to the dislocation lines. Hence, the spacing between Moiré fringes is half the spacing between dislocations for $\bar{2}$00 and 020 operating reflections (Fig. 6c and 6d respectively.

From the mean spacing of the Moiré fringes in Fig. 6a to d the misfit between the lattice can be calculated [14,15]. The

results are shown in Table I, where $\varepsilon = (a_\beta - a_\gamma)/a_\beta$ is the misfit parameter. In addition from the spacing D between the dislocations ($D \approx 40$ nm) the misfit parameter can also be estimated [15], this gives:

$$\varepsilon = \frac{b}{D} \approx 7.5 \times 10^{-3}$$

where $b = a_\beta = 0.299$ nm [16], in good agreement with the misfit parameter obtained from the Moiré fringes spacing in Table I.

The lattice parameters of the β and γ phases in our alloy have not been measured. Nevertheless we can compare our results with those corresponding to the binary alloys (see Pearson [16]) which are shown in Table II. For the ternary alloy the misfit parameter could be expected to lie in between those shown in Table II. This matches quite well with the results obtained from Moiré fringes and dislocation spacing in Table I.

It is concluded that the precipitates are essentially encircles by edge loops, with $b = a_\beta\langle 100\rangle$.

This result is different to that obtained by Stephens and Purdy [17] analyzing the γ-β interface in Cu-Zn alloys. These authors have concluded that the γ-precipitates were surrounded by a complex net of interfacial dislocations having a/2 $[\bar{1}\bar{1}0]$, a $[\bar{1}00]$ and a/2 $[\bar{1}1\bar{1}]$ Burgers vectors. From the micrographs they have shown it is difficult to confirm such a conclusion. Nevertheless we can emphasize that our conclusion (the precipitates are only encircled by <100> edge dislocation loops) is consistent with the micrographs (Fig. 3) of Stephens and Purdy; but their conclusion is in disagreement with our results of Fig. 6, i.e., the extinctions observed in Fig. 6 cannot be

explained if a/2 <111> type Burgers vector is assumed. Moreover, if the lines observed in Fig. 3 in the paper of Stephens and Purdy are assumed to be Moiré fringes a mean spacing of about 160 nm is found. The lattice misfit calculated from this spacing gives $\varepsilon \quad 1.3 \times 10^{-3}$ which is rather close to the value given in Table II for Cu-Zn. Using this misfit parameter the distance between the edge dislocations is expected to be $D = \frac{b}{\varepsilon} = 230$ nm, where $b = a_\beta$ was assumed. This is nearly the spacing between the vertical segments (which could be related to the line directions of <100> edge dislocations) in Fig. 3a of Stephens and Purdy [17].

CONCLUSIONS

The kinetics for the growing of the γ-precipitates follows the Ostwald ripening mechanism. This is evident from the linear relationship between $\bar{r}^3$ and t^*, and the asymmetry in the size distribution.

The shape of the precipitates evolves from cuboidal with {100} habit when they are smaller to polyhedral with {100} and {110} facets when they are bigger.

The precipitates are fully coherent with a vacancy type of stress field at the first stages but become semicoherent for larger sizes. In the latter case the precipitates are encircled by a <100> edge type dislocation loops. The lattice misfit between matrix and precipitates was determined from both dislocations spacing and Moiré fringes spacing, the results are consistent giving for the misfit parameter $\varepsilon = 7 \times 10^{-3}$.

Acknowledgments: One of the author (F.C.L.) acknowledges the DGICy T of Spain for financial support during his stay in the Universitat de les Illes Balears, where this work was carried out.

REFERENCES

1. R. Rapacioli and M. Chandrasekaran, Proc. Int. Conf. Martensitic Transformations, (Cambridge MA, USA), 1979, p.596.
2. C. Auguet, E. Cesari, R. Rapacioli and Ll. Mañosa, Scripta Metall. 23 (1989) 585.
3. J. Pons and E. Cesari, Thermochim. Acta, 145 (1989) 237.
4. F.C. Lovey, E. Cesari, C. Auguet, Ll. Mañosa, and R. Rapacioli, Proc. Int. Conf. Martensitic Transformations (Sydney, Australia), 1989, in press.
5. R. Rapacioli, M. Chandrasekaran and F.C. Lovey, Proc. Int. Conf. Solid-Solid Phase Transformations (Pittsburg, USA), 1981, 739.
6. F.C. Lovey, R. Rapacioli and M. Chandrasekaran, Phys. Stat. Sol (a), 68 (1981) K105.
7. F.C. Lovey, G. Van Tendeloo, J. Van Landuyt, M. Chandrasekaran, and S. Amelinckx, Acta Metall. 32 (1984) 879.
8. G. Van Tendeloo, M. Chandrasekaran, and F.C. Lovey, Metall. Trans. A, 17 (1986) 2153.
9. G. Van Tendeloo, M. Chandrasekaran, and F.C. Lovey, Proc. ICOMAT 86 (Nara, Japan) (1986) 868.
10. J.M. Lifshitz and V.V. Slyozov, J. Phys. Chem. Solids, 19 (1961) 35.
11. C. Wagner, Z. Flektrochem. 65 (1961) 581.
12. H. Yamauchi and D. De Fontaine, Acta Metall. 27 (1979) 763. A.G. Kachaturyan, S.V. Semenovskaya and J.W. Morris Jr., Acta Metall. 36 (1988) 1563.

13. A.K. Head, M.H. Loretto, and P. Humble, Phys. Stat. Solidi, 20 (1967) 505.

14. R. Gevers, Phil. Mag., 7 (1962) 1681.

15. P.b. Hirsh, A. Howie, R.B. Nicholson, D.W. Pashley, and M.J. Whelan, Electron Microscopy of Thin Crystals (Butterworths, London) 1965, p.343.

16. W.B. Pearson, Handbook of Lattice Spacing and Structure of Metals. Metal Physics and Physical Metallurgy (ed. G.V. Raymar) V.8 (1967).

17. D.E. Stephens and G.R. Purdy, Acta Metall. 23 (1975) 1343.

FIGURE CAPTIONS

Fig. 1: Bright field electron micrograph of γ-type precipitates in the as quenched state.

Fig. 2: a) Precitates after flash heating to 673 K for 20s.

b) The corresponding size distribution.

Fig. 3: a) Precipitates after flash heating to 673 K for 40s.

b) The corresponding size distribution

Fig. 4: a) Precipitates after flash heating to 673 K for 60s.

b) The corresponding size distribution.

Fig. 5: a) Precipitates after flash heating to 673 K for 100s

b) The corresponding size distribution.

Fig. 6: a) to d) Contrast analysis of Moiré fringes and interface dislocations. The precipitates are encircled by <100> type edge dislocation loops.

Fig. 7: Relationship between $\bar{r}^{-3}$ and the ageing time t^{*}.

TABLE I

Diffraction vector g	Moiré fringes spacing Δx [nm]	$\varepsilon = 1/g\ \Delta x$
$<110>/a_\beta$	31.0	6.4×10^{-3}
$<200>/a_\beta$	20.8	7.1×10^{-3}

Moiré fringes spacing and misfit parameters for the 110 and 200 diffraction vectors.

TABLE II

	Lattice parameters [nm]		Misfit Parameter
	β-Phase {100}	γ-Phase {300}	ε
Cu-Zn	0.29539	0.29533	2×10^{-3}
Cu-Al	0.29564	0.29013	18×10^{-3}

Lattice and misfit parameters of the β and γ phases in Cu-Zn and Cu-Al alloys

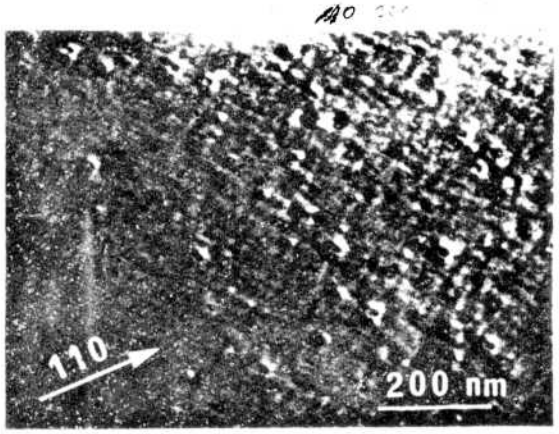

Fig. 1

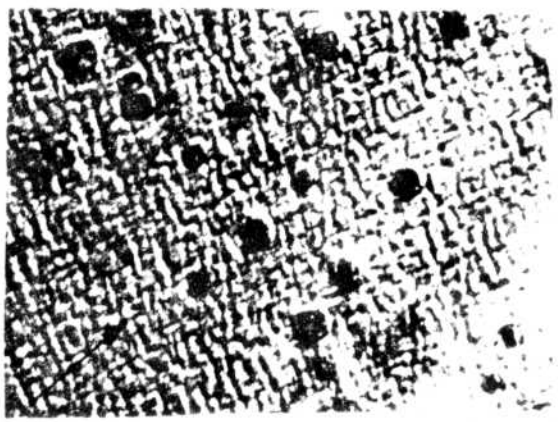

Fig. 2a

Fig. 3a

Fig. 4a

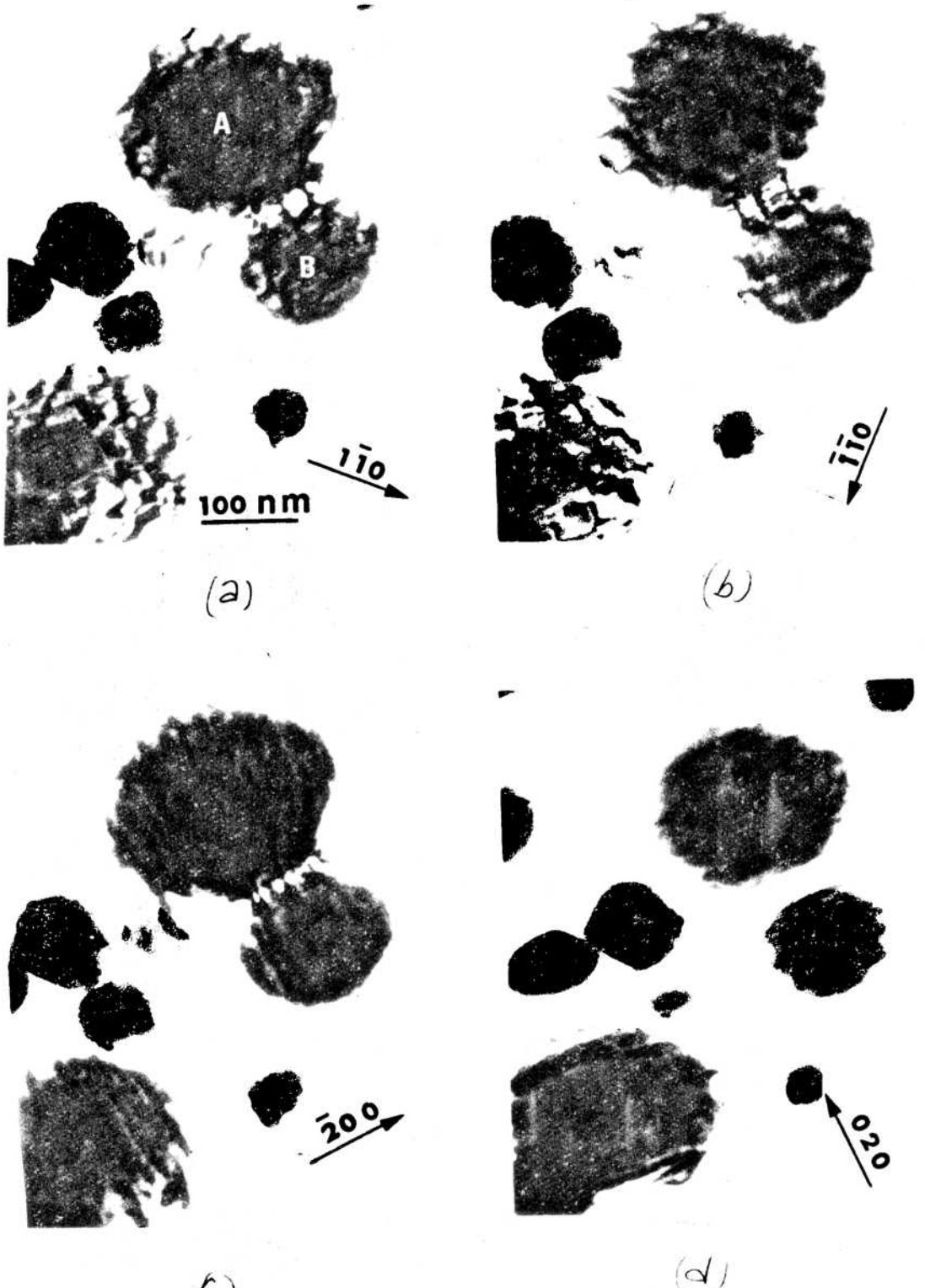

Fig. 6

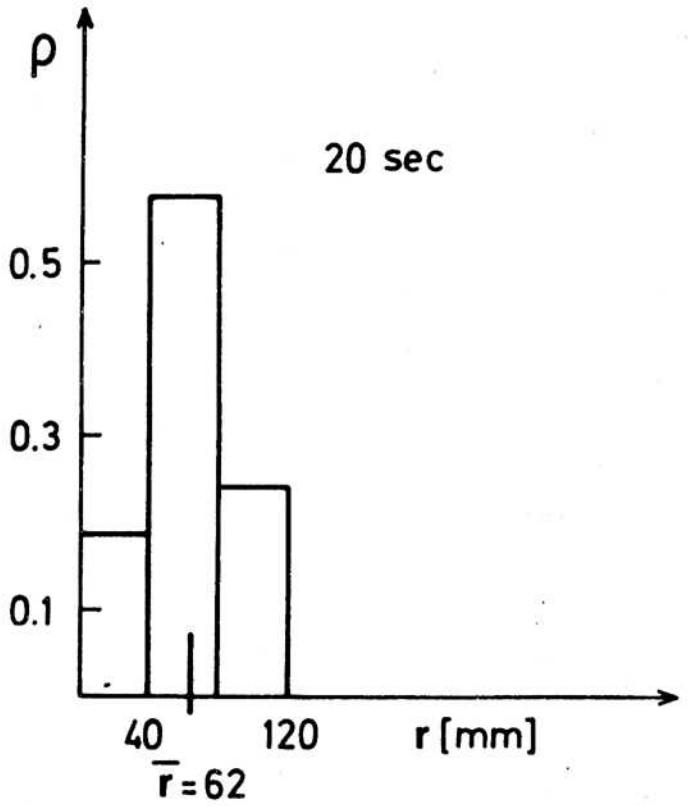

Fig 2 b

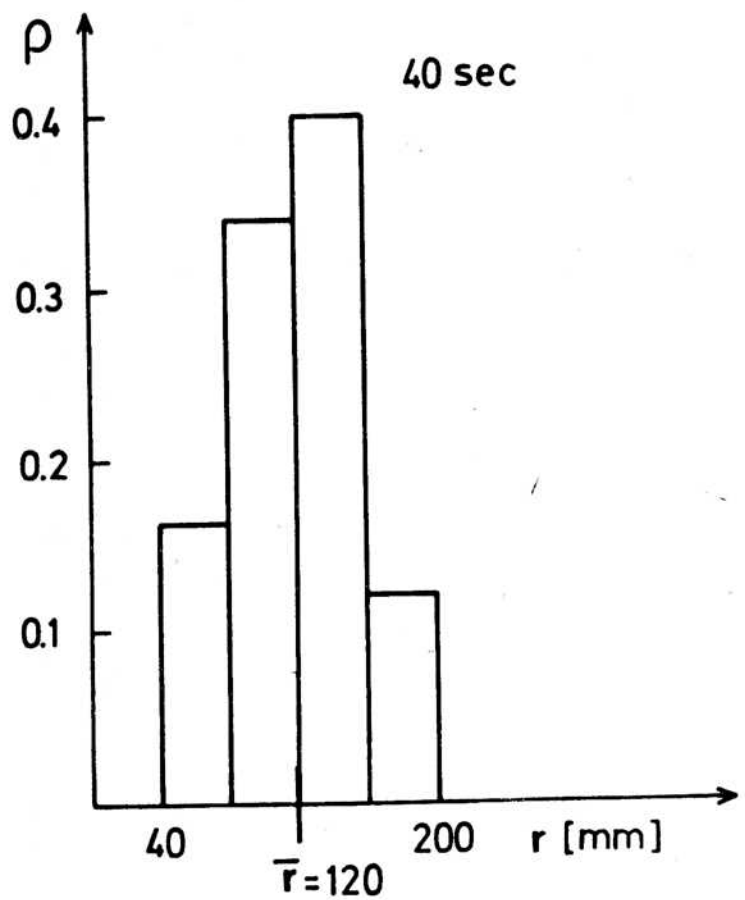

Fig. 3 b

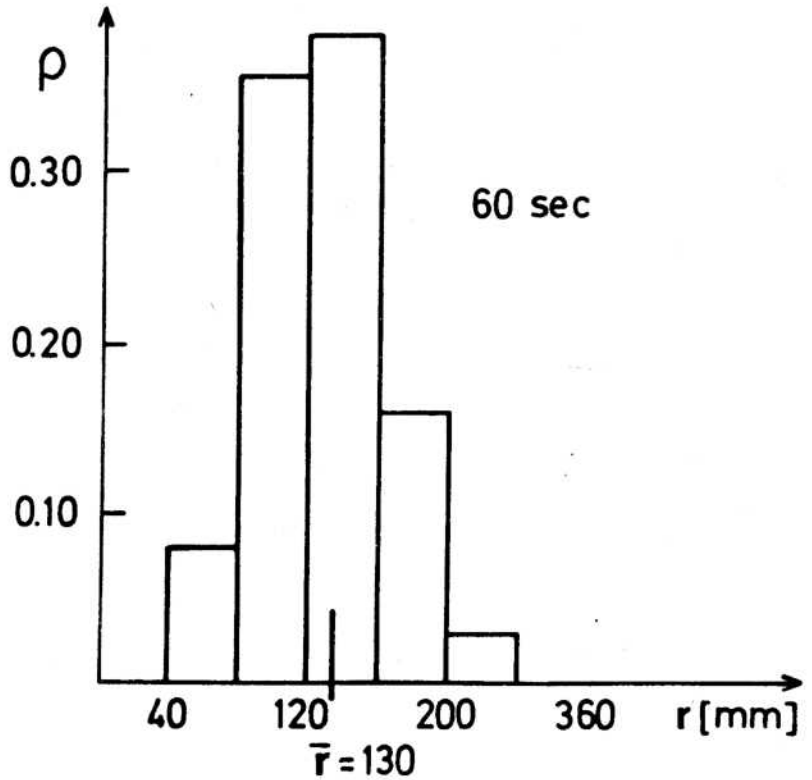
ρ
0.30
0.20
0.10
60 sec
40
120
200
360
r [mm]
r̄ = 130

Fig. 4 b

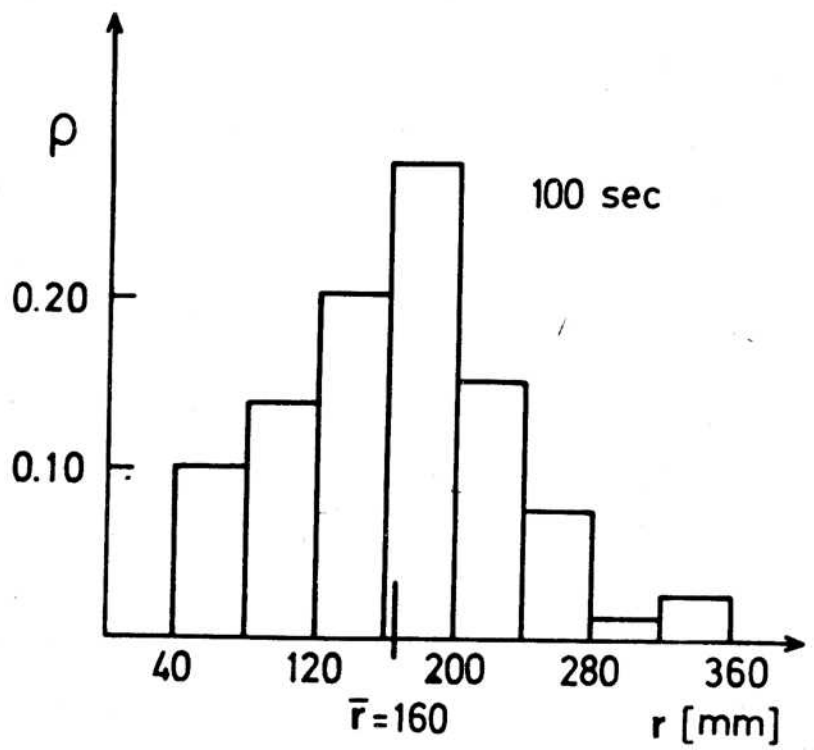
ρ
0.20
0.10
100 sec
40
120
200
280
360
r̄ = 160
r [mm]

Fig. 5 b

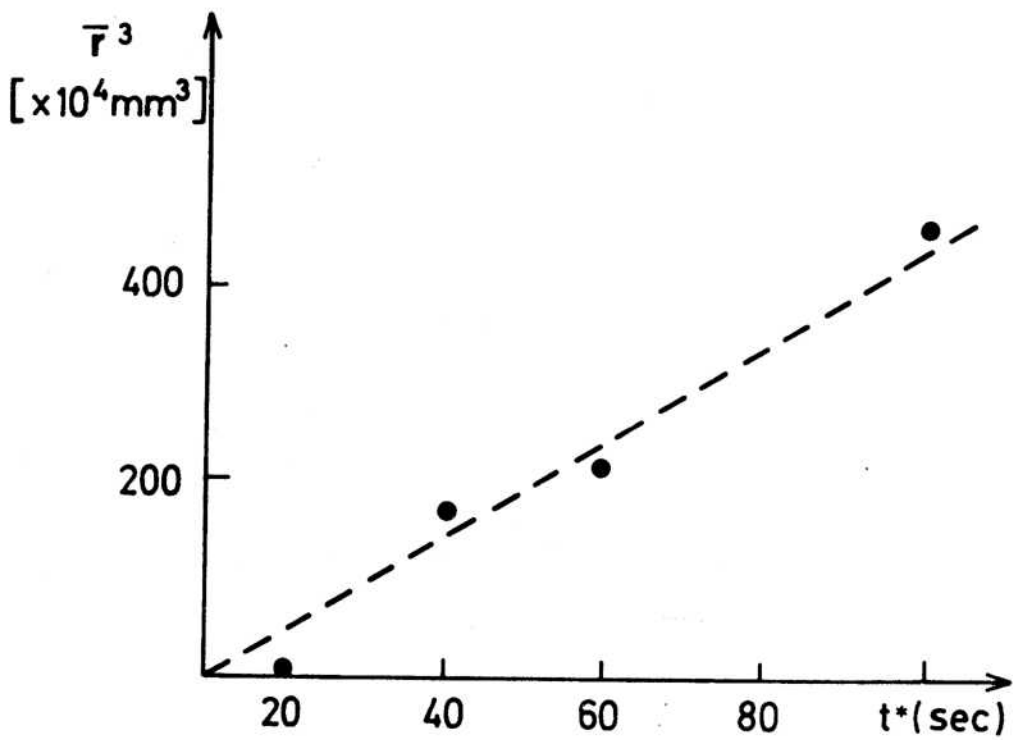

Fig. 7